

Ionic Diode-Based Drug Delivery System

Hyunjae Yoo, Soon-Bo Kang, Jeongsoo Kim, Wonkyung Cho, Hyojeong Ha, Seyoung Oh, Seol-Ha Jeong, Sihwan Lee, Hyemin Lee, Chang Seo Park, Dong-yup Lee, Taek Dong Chung,* Kyung-Mi Lee,* and Jeong-Yun Sun*

Drug delivery systems hold promise for delivering cytotoxic drugs by controlling the timing and location of the drug release. However, conventional delivery mechanisms often fall short of achieving spatiotemporally controlled yet sustained release, which is crucial for ensuring drug efficacy and minimizing impact on surrounding tissues. Here, an ionic diode-based drug delivery system is reported that is controlled by an electric potential and capable of releasing drugs at scales ranging from nanogram to microgram. The migrated drug is slowly but continuously diffused to the lesion through the hydrogel at the desired rate. The ionic diode provides flow-free drug delivery while minimizing unintended drug leakage over prolonged periods. Implanted in a freely moving tumor-bearing mouse model, the system filled with doxorubicin demonstrated superior anti-tumor efficacy and minimal off-target immune toxicity compared to the intratumoral injection of free doxorubicin. With its mechanically compliant and biocompatible components, the system offers a safe and readily translatable approach to patients with surgically unresectable tumors.

1. Introduction

Drug delivery systems have gained interest over the past decades as the efficacy and safety of drugs are heavily reliant on how they are administered.^[1] For example, after the injection of a single large dose, the plasma concentration of a drug initially elevates above the minimum toxicity concentration (MTC) and then rapidly drops below the minimum effective concentration (MEC).^[2] To treat localized diseases, a lesion-specific and timely drug release strategy that can maintain the plasma concentration of a drug between MEC and MTC for an extended period is highly recommended.^[3] Active drug delivery systems hold promise for treating these diseases by providing user-defined, programmable control over the timing and location of drug release.^[4] Ideally, such systems would combine the following features: 1) sustained release system that is spatiotemporally controlled without

generating unintended pressure on tissues, thus reducing adverse effects; 2) a composition that is soft, flexible, stretchable, and biocompatible, ensuring safe interaction with human tissue; and 3) an implantable system with low power consumption for long-term, patient-friendly usage.^[3,5]

To accomplish these features, the trigger mechanisms have varied widely. Stimuli-responsive systems, typically based on magnetic fields,^[6] electric current,^[7] electromagnetic radiation,^[8] thermal stimuli^[9] and photons,^[4,10] offer intrinsic sustained release and biocompatibility without internal power consumption. Nevertheless, they tend to fall short in providing on-off switchable, on-demand, and directional control of drug release. They can also induce issues with the stimuli methods themselves, as they generate heat in the media and require bulky external facilities.^[3] On the other hand, actuation-based systems, which utilize electrochemical actuation^[11] or micromachines,^[12] offer enhanced spatiotemporal control of drug release. However, they often lack softness, flexibility, and stretchability when implanted for prolonged therapy. Moreover, they inevitably cause hydrodynamic damage to nearby tissues as they rely on mechanical pressure to squeeze out the aqueous drug solution from the reservoir.^[13]

Iontronics has attracted considerable attention for its capability to actively deliver discrete ion doses to precise locations

H. Yoo, S.-B. Kang, S. Lee, C. S. Park, D.-yup Lee, J.-Y. Sun
Department of Material Science and Engineering
Seoul National University
Seoul 08826, Republic of Korea
E-mail: jysun@snu.ac.kr

J. Kim, H. Ha, S. Oh, H. Lee, K.-M. Lee
Department of Biochemistry and Molecular Biology
Korea University College of Medicine
Seoul 02841, Republic of Korea
E-mail: kyunglee@korea.ac.kr

W. Cho, T. D. Chung
Department of Chemistry
Seoul National University
Seoul 08826, Republic of Korea
E-mail: tdchung@snu.ac.kr

S.-H. Jeong
School of Chemical and Biological Engineering
Institute of Chemical Processes
Seoul National University
Seoul 08826, Republic of Korea

J.-Y. Sun
Research Institute of Advanced Materials (RIAM)
Seoul National University
Seoul 08826, Republic of Korea

The ORCID identification number(s) for the author(s) of this article can be found under <https://doi.org/10.1002/adma.202412377>

DOI: 10.1002/adma.202412377

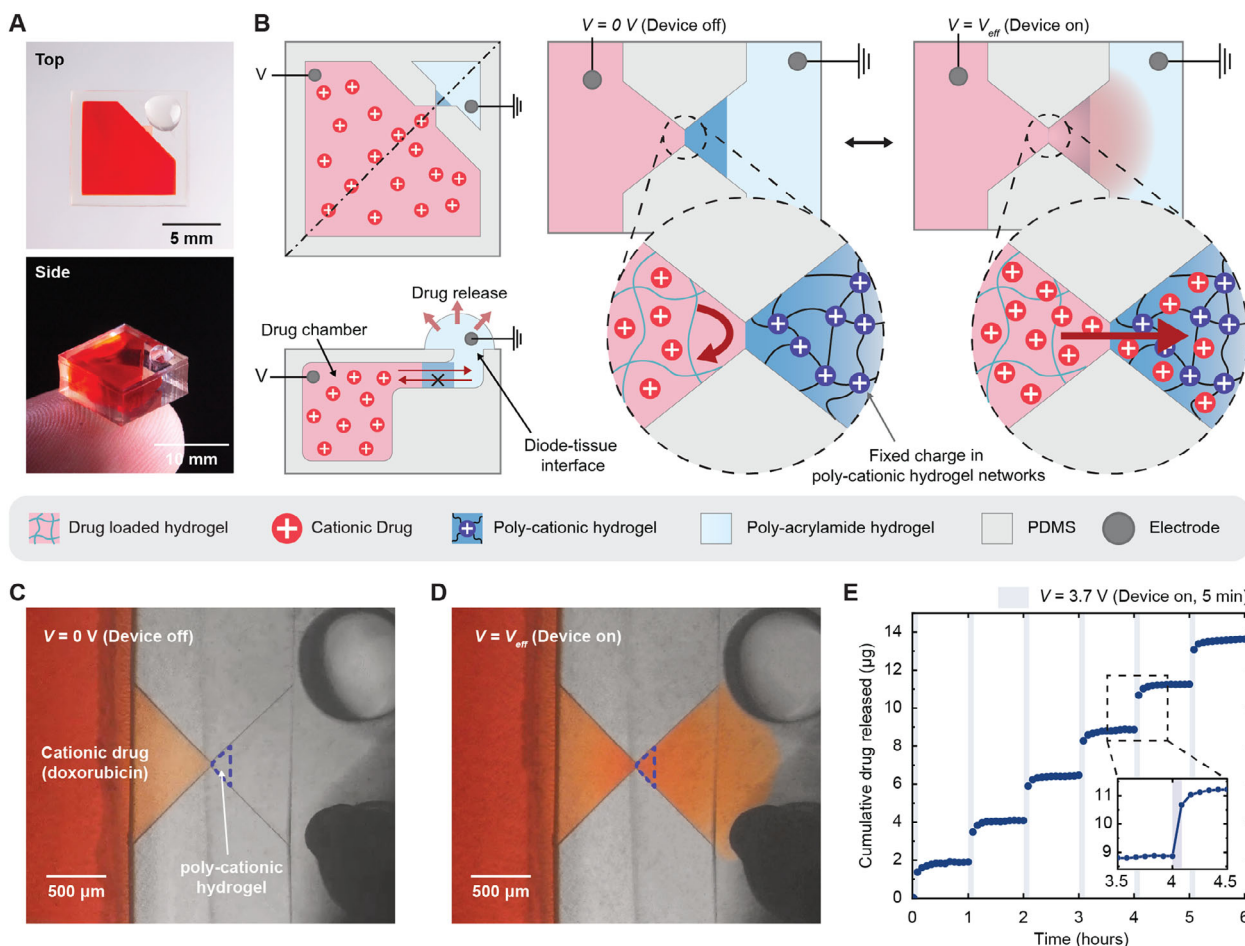


Figure 1. Flow-free, spatiotemporally controlled, soft, implantable Ionic diode-based Drug Delivery System (IDDS). A) Photograph of IDDS. B) The operation principle of IDDS. Without electric potential ($V = 0$), poly-cationic hydrogel networks repel the diffusion of cationic drugs. The drugs pass through the poly-cationic hydrogel only when an effective electric potential V_{eff} is applied. C) Photograph of IDDS using doxorubicin (red, DOX) as a cationic drug after immersed in DPBS for 24 h. D) The device after 5 min of +3.7 V electric potential. DOX moves from left to right, crossing the poly-cationic hydrogel. Scale bar: 500 μm . E) Cumulative amount of DOX delivered after on-off cycles. The device is on for 5 min at +3.7 V and off for 55 min at 0 V every hour.

at desired moments.^[14] Ionic diodes stand out from iontronics due to their ability to accurately transport ionic charge carriers without hydrodynamic pressure.^[15] They enable unidirectional ion transport by applying an external electric field across ion exchange membranes with an asymmetric structural design called a heterojunction.^[16] However, for ionic diodes to be applicable in drug delivery systems, they need to control relatively larger drug molecules beyond their typical targets, such as small ions (K^+ , Na^+ , and Ca^{2+}) or neurotransmitters (glutamate, dopamine, and GABA).^[17] Furthermore, despite significant progress, ionic diodes still face challenges regarding biocompatibility, softness, flexibility, and stretchability, which complicate their use in implantable drug delivery systems.

Herein, we report a flow-free, spatiotemporally controlled, soft, and implantable ionic diode-based drug delivery system (IDDS) (Figure 1A). By introducing a poly-cationic hydrogel-based ionic diode, which acts as an on-off gate controlled by an electric potential, our system provides precise drug release without hydrodynamic pressure. The ionic diode migrates a drug in a timely man-

ner, and the migrated drug is slowly but continuously diffused to the lesion through the hydrogel. Without further action, our system shows minimal leakage over prolonged periods. To achieve in vivo affinity – softness, flexibility, stretchability, and biocompatibility of the system –, poly-dimethylsiloxane is utilized as an encapsulation material. Moreover, to control drugs with high molecular weight, the mobility of the drug is tuned by embedding it into the hydrogel matrix. Long-term in vivo experiments of programmed drug delivery in freely moving mouse models demonstrate sustained drug release function, which suppresses tumor volume while minimizing damage to immune cells.

2. Results and Discussion

2.1. Design and Mechanism of the System

IDDS is designed to incorporate an hourglass-shaped ionic diode with three types of hydrogels (Figure 1A,B).^[18] Poly-cationic hydrogel is a key component of ionic diode which

operates as an on-off gate controlled by an external electric field. By utilizing an hourglass-shaped poly-cationic hydrogel, electric potential drops predominantly at the junction.^[19] The concentrated electric potential makes it possible to control a drug with high molecular weight with only a few voltages. In the drug chamber, cationic drug is stored in a 3 M poly-acrylamide hydrogel to match the mobility of the drug through the device. Diode-tissue interface is composed of biocompatible poly-acrylamide hydrogel, which ensures sustained drug release and gentle contact with tissues. All the hydrogel structures except diode-tissue interface are encapsulated with polydimethylsiloxane (PDMS) to ensure biocompatibility. Ag/AgCl electrodes are used for both cathode and anode to exclude undesired electrochemical reactions and to minimize an impedance at the interface between electrodes and electrolytes.^[18] The detailed structures and compositions are described in the experimental section.

The operation mechanism of IDDS is summarized in Figure 1B. At off state (Voltage = 0 V), positively charged ions fixed in poly-cationic hydrogel repel diffusion-based cationic drug movement (Figure 1B middle). The leakage test without applied voltage verifies near-zero leakage of the device over an extended period (Figure S1, Supporting Information). When effective electric potential (Voltage = V_{eff}) is applied to the electrodes, cationic drugs penetrate through poly-cationic hydrogel by electrophoretic force (Figure 1B right). Unlike traditional convection-based systems, the mechanism does not generate hydrodynamic pressure at the diode-tissue interface as it relies on electrophoresis and concentration-dependent diffusion. As we can see in Figure 1C, a cationic drug doxorubicin (DOX, red) stays in the drug chamber when an external electric field is zero. The drug progressively moves through the poly-cationic hydrogel when V_{eff} is applied to the electrodes (Figure 1D; Movie S1, Supporting Information).

The drug delivery property of the device is demonstrated through on-off cyclic tests (Figure 1E). Each cycle consists of 5 min at +3.7 V followed by 55 min in the off state, and the cumulative amount of the drug is measured every 5 min by using a UV-Vis spectrometer. The graph exhibits that the device has an inherent capability for accurate on-demand control and sustained release. The detailed process is depicted in the experimental section and Figure S2, Supporting Information.

2.2. Fabrication Process of IDDS for Delivery of Heavy Cationic Drugs

To optimize the ionic diode system for a drug delivery, hydrogels are sequentially patterned on the device by UV photopolymerization (Figure 2A). Initially, a benzophenone (BP) and triphenylphosphine (TPP) treatment followed by an oxygen plasma treatment is applied to improve an adhesion at the hydrogel-PDMS interface.^[20] Subsequently, the hydrogels undergo UV polymerization in three steps: 1) A 100 μm of poly-cationic-acrylamide (DADMAC: Acrylamide = 3 M: 1 M) random copolymer hydrogel first networks are polymerized at the junction. 2) After removing the remaining solution, 3 M acrylamide hydrogel precursor solution is soaked for 3 min. Then the solution is UV polymerized to reinforce the mechanical properties of the

poly-cationic-acrylamide hydrogel by making poly-cationic interpenetration (CIPN) hydrogel. The stress-strain curves of the hydrogels show the enhanced mechanical property of CIPN hydrogel compared to pure poly-cationic hydrogel and poly-cationic-acrylamide random copolymer hydrogel (Figure S3, Supporting Information). Diode-tissue interface hydrogel is also polymerized at this step. 3) After removing the remaining solution, 3 M poly-acrylamide hydrogel with DOX is polymerized in the drug chamber to store the drug safely and to tune mobility. As the monomers and crosslinkers in the hydrogel precursor solution are known to be cytotoxic, the fabricated device is immersed in DPBS solution for over 24 h to remove any residuals. To confirm the absence of residual cytotoxic materials, in-vitro cell viability assay and live/dead cell assay using human dermal fibroblasts (HDF) are conducted on the DPBS solution after an additional 24-h immersion (Figures S4 and S5, Supporting Information). Moreover, nuclear magnetic resonance (NMR) spectroscopy analysis is conducted on the distilled water after an additional 24-h immersion to verify the absence of any residual monomers or crosslinkers in the device (Figure S6, Supporting Information). Both the cell viability assays, and NMR spectroscopy indicated that there are no detectable cytotoxic residues in the device. Notably, implantation tests of the device in wild-type C57BL/6 mice showed no signs of inflammation, weight changes, or peripheral immune toxicity, further reconfirming the absence of residual monomers or crosslinkers (Figures S7–S10, Supporting Information). The detailed fabrication sequences are described in the methods section.

The mobility of the drug in the ionic diode is tuned to overcome a challenge of its high molecular weight (Figure 2B,C). Traditional ionic diode systems have struggled with delivering heavy molecules, as depicted by an aggregation of DOX at the hydrogel junction under a +3.7 V electric potential (Figure 2B). The huge difference of drug mobility in aqueous solution and in poly-cationic hydrogel networks make the drugs to be aggregated at the junction. By embedding the drug into poly-acrylamide hydrogel, however, the issue is mitigated (Figure 2C). To verify the phenomenon, the electric mobility of DOX in an aqueous solution and various hydrogels is measured (Figure 2D). While the electric mobility of DOX in hydrogels is measured by electrophoresis experiment, that in aqueous solution is calculated by Einstein-smoluchowski relation,

$$\mu_q = \frac{Dq}{k_B T} \quad (1)$$

where μ_q is the electric mobility of the particle, D is the diffusion coefficient, q is the charge of the particle, k_B is the Boltzmann constant, and T is the absolute temperature, respectively. By substituting $5.83 \times 10^{-10} \text{ m}^2/\text{s}$ for the D of DOX in aqueous solution at 300 K,^[21] the calculated electric mobility of DOX in aqueous solution is $\approx 2.27 \times 10^{-8} \text{ m}^2/\text{s}$. The measured mobility and electrophoresis results quantitatively validate the schematic illustration, demonstrating that DOX moves 210 times faster in an aqueous solution compared to the CIPN hydrogel. Conversely, this mobility disparity drastically reduced to only 13 times when comparing the poly-acrylamide hydrogel used in the drug chamber to CIPN hydrogel.

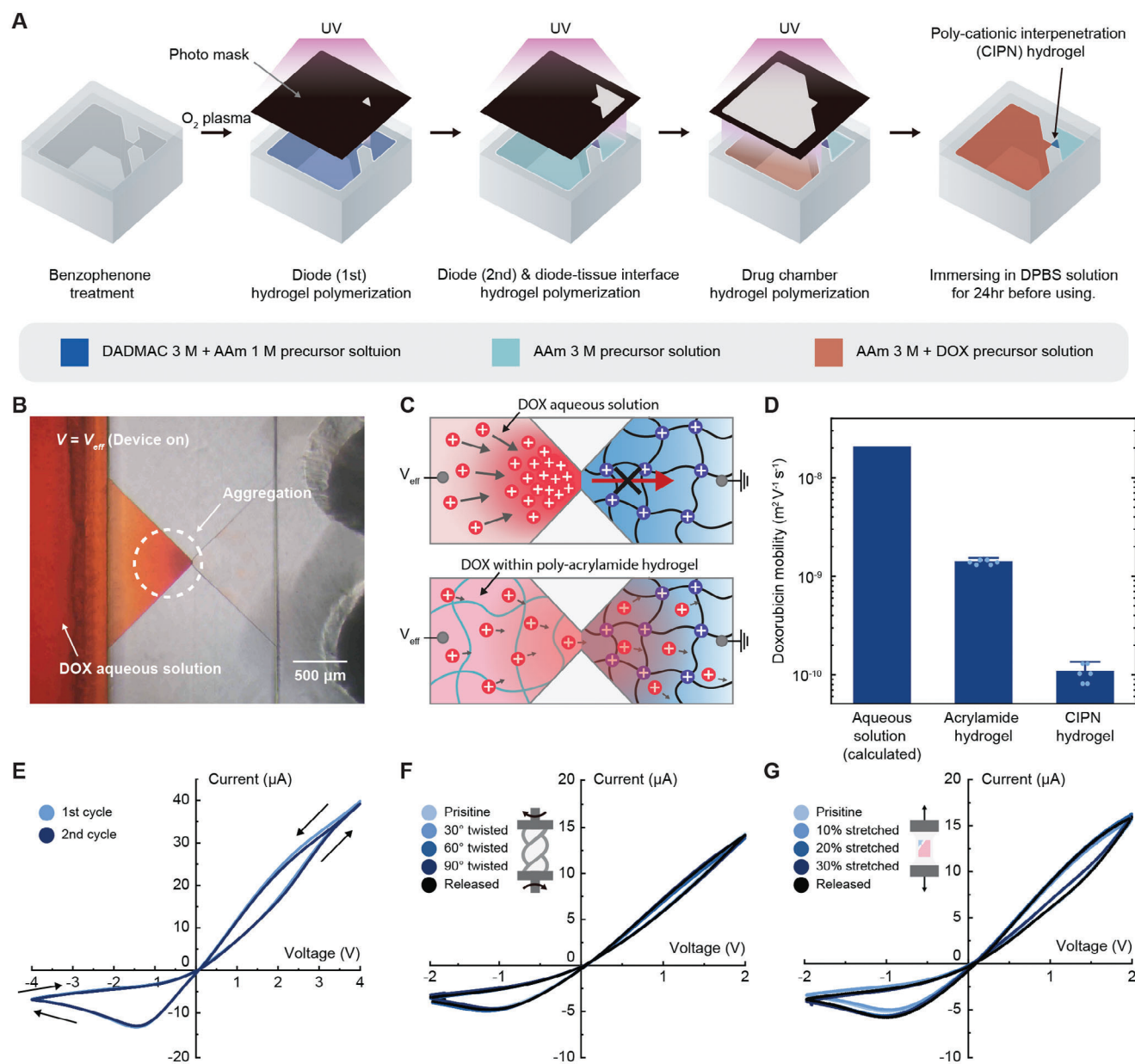


Figure 2. Fabrication process of IDDS for delivery of heavy cationic drugs and electro-mechanical stabilities of the device. A) Following benzophenone and O_2 plasma treatment on PDMS, hydrogels are UV polymerized in three steps. First, a poly-cationic-acrylamide hydrogel (DADMAC: acrylamide = 3 m: 1 m) is copolymerized at an hourglass-shaped junction to form the first networks of the ionic diode. Second, after removing the remains and soaking in 3 m acrylamide precursor solution for 3 min, a 3 m acrylamide hydrogel is polymerized. The polymerization covers both the diode region and the diode-tissue interface. Through successive polymerization, a poly-cationic interpenetration (CIPN) hydrogel is polymerized at the junction. Third, after removing the remains, a 3 m poly-acrylamide hydrogel with DOX is polymerized within the drug chamber. B) DOX delivery with a DOX aqueous solution, demonstrating the aggregation near the junction at +3.7 V electric potential. C) Schematic illustration of DOX delivery near the junction with DOX aqueous solution (top) and DOX within the poly-acrylamide hydrogel (bottom). D) The differences in DOX mobilities in aqueous solution, 3 m acrylamide hydrogel, and CIPN hydrogel. E) I - V curves from two consecutive cyclic voltammetry of IDDS. F) I - V curves of IDDS when twisted from initial state to a 90-degree angle and released. G) I - V curves of IDDS when stretched from the initial state to 30 percent strain and then relaxed. The scan rate for all cyclic voltammetry is 10 mV s^{-1} .

2.3. Characterization of the Electro-Mechanical Properties of IDDS

To analyze the electrochemical performance of the device, direct current (DC) voltage is applied to the device. Due to the geo-

metrical structure and the ion exchange features of poly-cationic hydrogel, the device exhibits stable ion current rectification.^[15] Two consecutive cycles of current-voltage (I - V) curves from -4 to +4 V of the device show its stability with rectification ratio of 5.90 (Figure 2E). The rectification behavior of the device under the

alternating cycle between 5 min of a +3.7 V forward bias and a -3.7 V reverse bias is shown in Figure S11 (Supporting Information), achieving a peak rectification ratio up to 17.92.

I-V curves of the device under conditions of twisting and stretching are measured to validate the flexibility and stretchability of it, respectively (Figures 2F,G; Figure S12, Supporting Information). The device consistently shows similar rectification behavior during and after being subjected to mechanical deformations. Remarkably, even when twisted by 90 degrees, the device preserves 98.33% of its initial rectification ratio. Similarly, it maintains 86.70% of its rectification ratio after being stretched by 30%. These results confirm the capability of device to retain stable electrical performance under extreme mechanical conditions, an essential feature for implantable devices which should withstand the movements of nearby skins and muscles.

2.4. Drug delivery Properties of IDDS

Drug releasing properties of IDDS are demonstrated by DOX (5 mg ml⁻¹ diluted in poly-acrylamide hydrogel). Following each operation cycle described in the insets of Figure 3C,F,G, an amount of DOX delivered per cycle is analyzed via optical UV-VIS spectroscopy at an absorption peak ($\lambda = 485$ nm.^[22] Reference data for the UV-VIS absorbance of DOX at $\lambda = 485$ nm is shown in Figure S13 (Supporting Information). A series of operations with device on time (t_{on}) ranging from 1 to 5 min are conducted to figure out the effect on DOX delivery and charge transfer per cycle (Figure 3A,B). The charge is measured by integrating the current between the working and counter electrodes. These operations follow the cycle diagram depicted in Figure 3C. As highlighted in Figure 3A,B, the device exhibits saturation in the amount of DOX and charge delivered after the third cycle. The profiles of the DOX and charge delivered post-saturation are depicted in Figure 3C. Similarly, a series of operations with effective voltage (V_{eff}) ranging from 1 to 4 voltages are conducted (Figure 3D,E). These operations follow the cycle diagram depicted in Figure 3F, and as with the previous experiment, the device shows saturation after the third cycle. The profiles of DOX and charge delivered post-saturation are depicted in Figure 3F. Figure 3A–F demonstrate that the amount and the rate of the DOX delivered are reliably correlated with t_{on} and V_{eff} , respectively. Since the drug release properties of IDDS depend on ion accumulation at the junction under the applied electric potential, drug release tests are conducted at various doxorubicin concentrations (Figure S14, Supporting Information).

As Ag/AgCl electrodes can be run out with a one directional bias, an alternative forward and reverse electric bias is necessary for long-term delivery. The cumulative charge shown in Figure 3G reveals that the electrodes can be restored by following the cycle, as the net charge after the cycle remains nearly zero. To verify the effect of the alternative electric potential on the drug delivery performance of the device, a series of operations following the cycle diagram in Figure 3G are conducted (Figures 3H,I). Unlike the results shown in Figure 3A–F, the profiles show consistent DOX delivery and charge transfer. Moreover, DOX delivered per cycle is reduced by 61.4% compared to the first cycle of Figure 3A, which has the same condition of forward bias: $t_{on} = 5$

min, and $V_{eff} = +3.7$ V. The reduced amount of DOX may stem from the reverse bias, as the transported DOX present in the PBS solution moved back into the device during the application of the reverse bias.

2.5. Assessment of In-Vivo Anti-Tumor Efficacy and Immune Toxicity of IDDS

DOX, a cytotoxic anthracycline, has been used for over three decades to treat both hematologic and non-hematologic malignancies. It functions by inhibiting topoisomerase 2, an enzyme crucial for DNA replication and cell division. We hypothesized that the sustained and on-demand release of DOX through IDDS could achieve effective tumoricidal effects while minimizing off-target immune toxicity.^[2,3,23]

To verify this hypothesis, we utilized an in-vivo tumor-bearing mouse model by implanting B16F10 melanoma cells subcutaneously into the right flank of the mice. Seven days after tumor inoculation, IDDS was implanted within the peritoneum, adjacent to the tumor mass (Figure 4A,B). The device was programmed to a 2-h cycle, allowing for 6 min of drug release under a +3.7 V forward bias and 55 min for electrode recovery under a -3.7 V reverse bias (Figure 4C; Table S1, Supporting Information). The electric potential was provided by a lithium-polymer battery and a wireless switch, both secured on the mouse with adhesive film dressings (Figure S15, Supporting Information). The current-time graph for the device during the operation cycle showed that both forward and reverse current remained constant after 72 h of operation (Figure S16, Supporting Information). The control groups received equivalent doses of DOX per day via direct intratumoral injection.

Our results indicate that tumor growth is significantly slower in the device-implanted groups receiving 6 $\mu\text{g day}^{-1}$ of DOX (136 ± 44.2 mm³ at D+17) compared to the 0 $\mu\text{g day}^{-1}$ control group (470 ± 31.5 mm³ at D+17) or those receiving 6 $\mu\text{g day}^{-1}$ of DOX intratumorally (271 ± 113 mm³ at D+17), resulting in over 70% decrease in tumor size by day 17. However, the device-implanted group receiving 2 $\mu\text{g day}^{-1}$ of DOX did not exhibit significant tumoricidal effect. At these DOX concentrations, the control groups receiving 2 or 6 $\mu\text{g day}^{-1}$ of DOX via intratumoral injection did not exhibit statistically significant tumor reductions, although there was a trend toward decreased tumor volumes (Figure 4D,E). This lack of significant reduction in the control groups may be attributed to necrosis of the skin and surrounding tissues caused by repeated intratumoral injection. Additionally, as the tumor size increased, uniform drug delivery became impractical, leading to considerable variability in tumor size within the group. DOX has fluorescence spectra with peak excitation (λ_{ex}) and emission (λ_{em}) wavelengths at 470 and 560 nm, respectively. We measured DOX accumulation using 488 nm laser and a 585/42 bandpass filter in flow cytometry (Figure S17, Supporting Information). Flow cytometry results revealed that while DOX fluorescence increased linearly with dose in the control groups, the device group exhibited a similar yet attenuated increase (Figure 4F). These data suggest that the reduced tumor growth in the device-implanted group was not directly associated with higher DOX-mediated killing of tumor cells, but rather with the indirect activation of tumor-infiltrated immune cells.

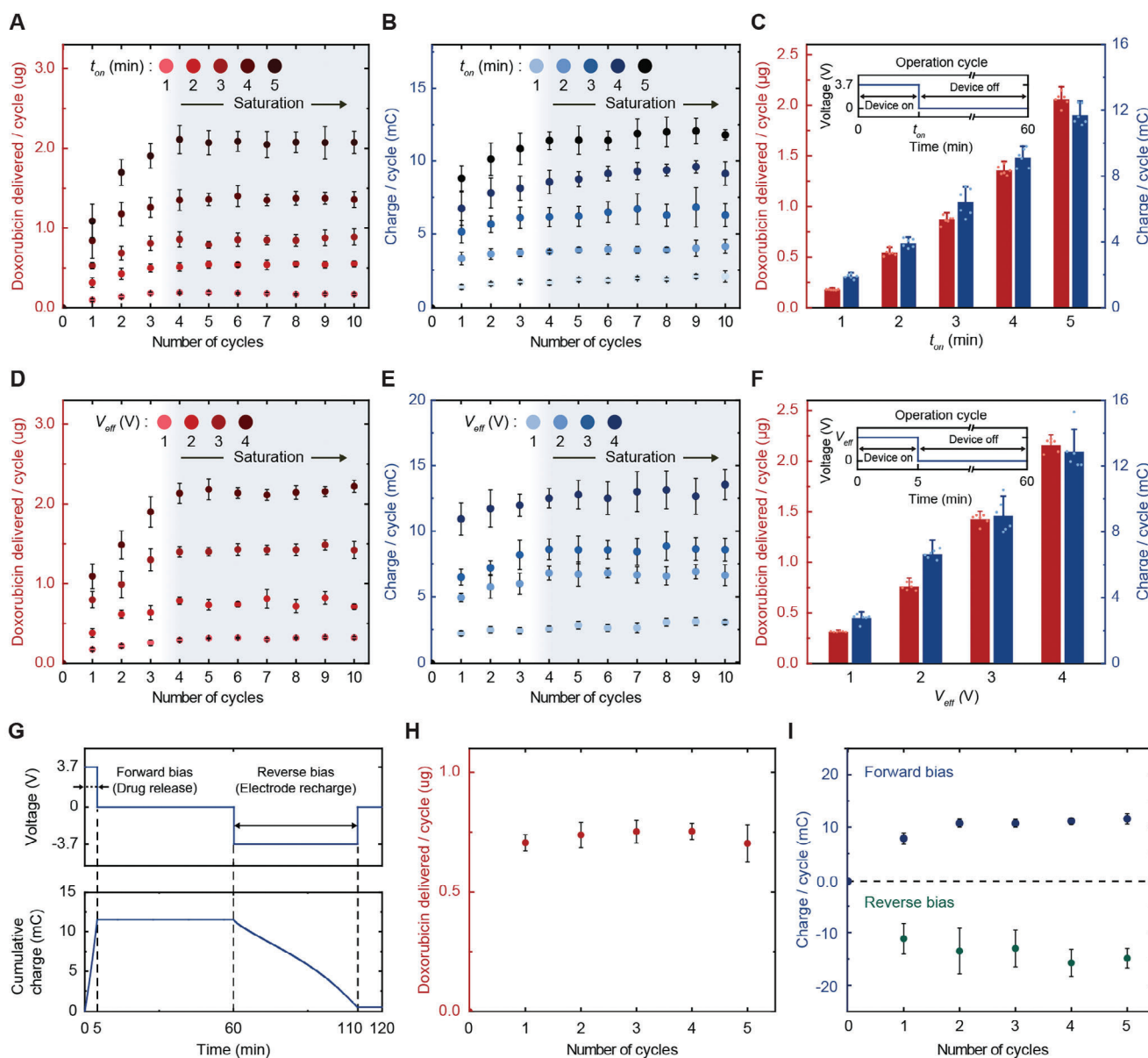


Figure 3. Drug delivery properties of IDDS. A,B) The amount of DOX (A) and charge (B) delivered by number of cycles with operation time (t_{on}) ranging from 1 to 5 min. C) Profiles of DOX and charge delivered by IDDS after saturation depicted in (A) and (B), with various t_{on} at +3.7 V electric potential. D,E) The amount of DOX (D) and charge (E) delivered by number of cycles with effective voltage (V_{eff}) ranging from 1 to 4 V. F) Profiles of DOX and charge delivered by IDDS after saturation depicted in (D) and (E), with various V_{eff} over a fixed duration of 5 min. G) Operation cycle diagram under ± 3.7 V forward-reverse alternating potential. H,I) Amount of DOX (H) and charge (I) delivered by the number of cycles described in (G). The operation cycles of (A and B) and (D and E) are shown in the insets in (C) and (F), respectively. Data are shown as means \pm standard deviation, sample size $n = 6$ for each group.

DOX can induce direct cell death of tumor cells and thereby elicit indirect immunogenic cell death^[24] through antigen-specific immune responses of CD8⁺ T cells. CD8⁺ T cells, a component of the adaptive immune system, are specialized killer cells responsible for lysing tumor cells. During immunogenic cell death, DOX induces apoptosis of tumor cells; the released neo-antigens are then taken up by antigen-presenting cells and tumor cells and presented to CD8⁺ T cells via major histocompatibility complex (MHC) class I. Activated tumor

antigen-specific CD8⁺ T cells recognize and attack tumor cells, secreting interferon gamma (IFN- γ) to activate nearby immune cells and releasing perforin and granzyme-b to perforate the tumor cell membrane and induce apoptosis.^[25] However, topoisomerase 2 also plays a crucial role in the rapid proliferation of T cells that have recognized tumor antigens.^[26] Consequently, the inhibition of topoisomerase 2 by DOX could lead to T cell death and impair the anti-tumor immune response.

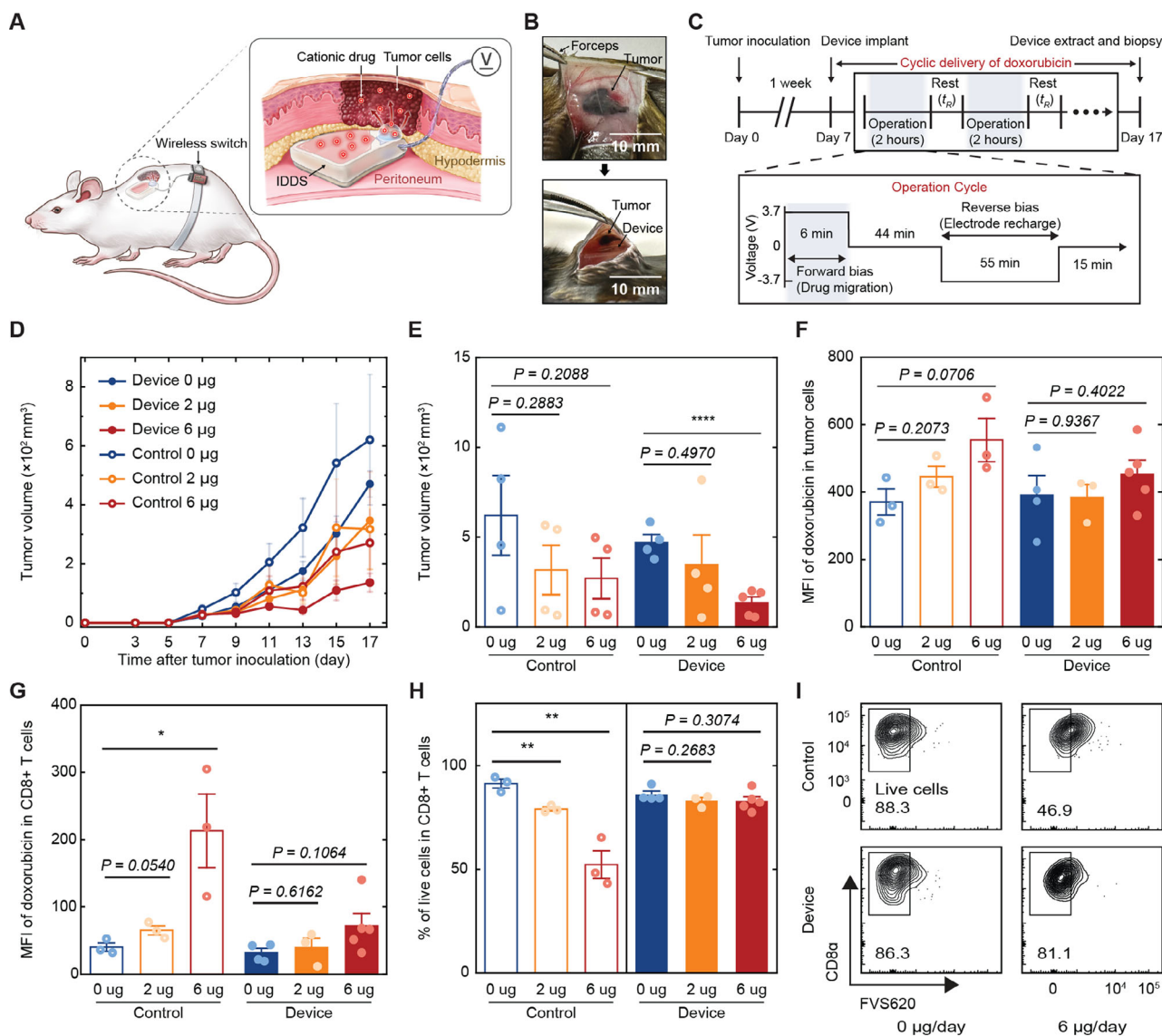


Figure 4. Assessment of in-vivo anti-tumor efficacy and immune toxicity of IDDS. A) Conceptual illustration of the in-vivo anti-tumor drug delivery system. B16F10 cells were subcutaneously inoculated into the right flank of mice, and IDDS was implanted between the peritoneum and tumor mass. B) Optical depiction of the device implantation procedure. C) Schematic representation of the experimental timeline and drug delivery cycle. $t_R = 0$ for 6 μg day⁻¹ and $t_R = 4$ h for 2 μg day⁻¹. D) Graph depicting B16F10 tumor growth in mice until day 17 with implanted IDDS and control mice. The control groups received the same dose of doxorubicin intratumorally. E) Tumor volume measured on day 17 after tumor inoculation. F) Mean fluorescent intensity (MFI) of doxorubicin in tumor cells. G, H) MFI of doxorubicin (G) and the proportion of live cells (H) in CD8+ T cells. I) Representative flow cytometry plots comparing the viability of CD8+ T cells between the control and IDDS-implemented groups receiving 6 and 0 μg day⁻¹. The numbers in the plots indicate the proportion of live cells within the total CD8+ T cell population. Data are shown as means \pm standard error of the mean. Significance was indicated as * $P < 0.05$; ** $P < 0.01$; **** $P < 0.0001$, and the statistical analysis was performed using unpaired Student's *t*-test.

To delineate the underlying mechanisms of the enhanced tumor suppression observed in IDDS-implemented groups, both DOX accumulation and viability of CD8+ T cells were assessed (Figure S18, Supporting Information). The viability of CD8+ T cells was analyzed by using Fixable Viability Stain 620 (FVS620), an amine-reactive dye that penetrates only dead cells.^[27] Flow cytometry analysis of CD8+ T cells revealed that although DOX fluorescence increased with dose in the control groups, the device-implemented groups exhibited a similar but significantly attenuated increase (Figure 4G).

The viability of CD8+ T cells appeared to be directly affected by DOX accumulation in the control groups. Specifically, CD8a+ cells in the control groups showed a marked shift toward the FVS620+ dead cell population in the 6 μg day⁻¹ group compared to the 0 μg day⁻¹ group, indicating DOX-induced CD8+ T cell death. In contrast, the device-implemented groups displayed minimal increase in DOX accumulation (Figure 4H, I), resulting in the protection of CD8+ T cells from DOX-induced killing and hence increased anti-tumor immunity.

Collectively, our experiments using a mouse melanoma model demonstrate that DOX delivery via IDDS exhibits superior anti-tumor efficacy and minimal off-target immune toxicity in tumor-bearing mice.

3. Conclusion

We have described an ionic diode-based drug delivery system and proved its potential use to precise, flow-free, sustained, and electrically controlled drug release for on-demand implantable therapy. The poly-cationic hydrogel-based ionic diode is central to our system, functioning as an on-off gate controlled by an electric potential. This design ensures nanograms to micrograms scale of drug migration and continuous diffusion to the lesion site without generating hydrodynamic pressure, a common limitation in conventional active drug delivery systems. The ionic diode also minimized unintended drug leakage over prolonged periods, which is critical for maintaining therapeutic efficacy and reducing side effects. The use of polydimethylsiloxane (PDMS) as an encapsulation material enhances the device's biocompatibility, flexibility, and stretchability, reducing the risk of adverse damage to surrounding tissues and improving patient comfort. The efficacy of our system was demonstrated through long-term in vivo experiments with freely moving tumor-bearing mouse models. Our system loaded with doxorubicin indicates higher viability in immune cells and suppression in tumor volume compared to intratumoral injection of free doxorubicin. Furthermore, as our device is not limited to the specific drugs or lesions, it shows promise as a universal drug delivery platform.

4. Experimental Section

Materials: Unless otherwise specified, the chemicals used in the current work were purchased from Sigma-Aldrich and used without further purification. For hydrogel polymer networks, Diallyldimethylammonium chloride (DADMAC; Sigma-Aldrich 32598) and acrylamide (AAm; Sigma-Aldrich A8887) were used as monomer. N,N'-methylenebisacrylamide (MBAAm; Sigma-Aldrich 146072) was used as crosslinker, while Lithium phenyl-2,4,6-trimethylbenzoylphosphine (LAP; Sigma-Aldrich 900889) was used as photoinitiator. For cationic drug, doxorubicin (DOX; Sigma-Aldrich D2975000) was used as anticancer drug. For elastomer treatment, benzophenone (BP; Daejung chemicals & metals 2633-4100) was used as photoinitiator and triphenylphosphine (TPP; Sigma-Aldrich T84409) was used as oxygen scavenger.

The elastomer substrate consisted of Sylgard 184 (polydimethylsiloxane, PDMS; Dow Corning MS-1003). Ag/AgCl electrodes were purchased from CHI Instruments. Kwik-Sil low toxicity silicone adhesive, used as a cover for the electrode during in-vivo test, was purchased from World Precision Instruments. Dulbecco's phosphate buffered saline (DPBS; Sigma-Aldrich D8537) was used as electrolyte.

Hydrogel Precursor Solution for IDDS: Unless otherwise indicated, the hydrogel was synthesized by dissolving DADMAC or AAm monomer with MBAAm and LAP with respect to the molar ratio of the monomer as crosslinker and photoinitiator, respectively, in DI water. For the poly-cationic copolymer hydrogel, a monomer solution containing 3 M DADMAC and 1 M AAm was mixed with 1.2 mol% of MBAAm and 0.05 mol% of LAP. For the diode-tissue interface hydrogel, a 3 M AAm monomer solution was mixed with 0.138 mol% of MBAAm and 0.0284 mol% of LAP. For the drug chamber hydrogel, 3 M AAm monomer solution was mixed with 1.495 mol% of MBAAm, 0.0567 mol% of LAP, and 5 mg mL⁻¹ DOX.

Fabrication of IDDS: PDMS was prepared by molding the mixture of base and curing agents (12:1 by weight) followed with a 60 °C treatment in an oven for 24 h. The top part with dimensions of 1 mm × 10 mm × 10 mm (height × length × width) without a pattern, is manufactured using a Petri dish. The bottom part with dimensions of 4 mm × 10 mm × 10 mm (height × length × width) is cured with SU-8 micropattern mold manufactured through photolithography. 50 μm height micropattern was built on hourglass-shaped junction and 300 μm height micropattern was built on both drug chamber and diode-tissue interface. In the case of the drug chamber, a 3 mm acrylic plate was additionally attached to the photolithography pattern to secure drug volume. Holes for injecting and removing solution into the channel were drilled using 1 mm bio-punch (KAI medical). Both the top and bottom part of PDMS were treated by oxygen plasma for 30 s (Covance-1 MPR; 610 mtorr, 180 mW) and attached in a 60 °C oven for 6 h.

PDMS microchannel was immersed for BP and TPP solution (20wt% BP and 4wt% TPP in ethanol) for 2 h to activate the surface.^[28] Then, the PDMS microchannel was cleaned with ethanol and completely dried in 60 °C oven. After all, the channel was treated by O₂ plasma for 30 s, same condition as PDMS-PDMS adhesion condition above, to form a hydrophilic surface to favor gelation in narrow channel. Poly-cationic copolymer hydrogel precursor solution was carefully poured on the PDMS microchannel and exposed to UV light (365 nm, 18 mW cm⁻²) for 14s (Karl Suss mask aligner MJB4). The PDMS microchannel was aligned under 100 μm UV photomask and subsequently exposed to UV light only in a limited area. Hydrogel forms chemical bond to the PDMS by directly curing hydrogel precursor onto the benzophenone absorbed PDMS surfaces.^[29] After gently removing the residue, acrylamide hydrogel precursor solution and cationic drug hydrogel precursor solution was poured in the diode-tissue interface and drug chamber, respectively. Acrylamide hydrogel precursor solution was exposed to UV light (365 nm, 18 mW cm⁻²) for 50 s. Acrylamide hydrogel was polymerized in diode-tissue interface region and polycationic copolymer hydrogel was reinforced by acrylamide double network. Then, poly-cationic drug hydrogel was polymerized by UV light (365 nm, 20 mW cm⁻²) for 1200 s. The holes were sealed firmly by Scotch tape (3M) during all hydrogel UV polymerization process written above. After the fabrication, IDDS was immersed in DPBS solution for over 24 hr to remove the residual monomers and fully swell the hydrogel.

In-Vitro Cell Viability Test: The in-vitro cell viability test was assessed using a cell proliferation assay (cell counting kit-8, CCK-8) and a live/dead assay. To analyze potential residuals in the device, the initial DPBS solution used for 24-h immersion was replaced with fresh DPBS, and the device was immersed for an additional 24 h.

Human dermal fibroblasts (HDF) cells were seeded into a 96-well plate at a density of 0.015 million cells per well. After 24 h of incubation, the medium was removed by suction, and the elution solution was mixed with 100 μL of cell media (high DMEM with FBS 10% p/s 1%) at a various ratio (cell media: elution solution = 10:1, 10:2, 10:3, 10:4, and 10:5) was added to each well. For the PBS group, fresh DPBS solution was mixed with cell media with the same ratios. The control group was incubated in the cell media without any additional mixing. The cells were incubated with the mixed cell media for an additional 24 h. Following the incubation, the cell media was removed, and 100 μL of the CCK-8 solution prepared by mixing serum-free DMEM with CCK in a 10:1 ratio was added to each well. The plate was protected from light by wrapping it in aluminum foil and incubated for 2 h. After incubation, 100 μL of the solution from each well was transferred to a 96-well plate, and absorbance was measured at 450 nm using a spectrophotometer.

Following the same protocol as the CCK experiment, HDF cells were prepared for the live/dead assay. A live/dead cell imaging kit (488/570), a sensitive two-color fluorescence assay for detecting cell viability with FITC and Texas red, was used. DMEM media was added to create a 2x stock solution, which was then added in equal volume to the cells. HDF cells were treated with the live/dead cell imaging kit for 15 min at room temperature. Live cells were stained green, while dead cells were stained red. The images were analyzed using a CLSM II confocal laser scanning microscope installed at the National Center for Inter-university Research Facilities (NCIRF) at Seoul National University.

Nuclear Magnetic Resonance (NMR) Spectroscopy: ^1H NMR spectra were collected on a 300 MHz NMR spectrometer (Avance III-300, Bruker). The elution solution was obtained by immersing the device in distilled water for an additional 24 h after washing. Each sample was dissolved in CDCl_3 for measurement. The 0 ppm reference for ^1H NMR was set using Tetramethylsilane (TMS), and the chemical shift of CDCl_3 was 7.26 ppm. The concentration of the sample was 1 w% of CDCl_3 .

In-Vivo Toxicity Test of IDDS: All animal experiments were approved by the Institutional Animal Care and Use Committee of Korea University (approval number: KUIACUC-2022-0002) and adhered to their guidelines and regulations. Wild-type (WT) C57BL/6 mice were purchased from Orient Bio. Inc. Female mice aged between 5 and 10 weeks were used. Mice were housed in a specific pathogen-free facility at Korea University.

Mice were implanted with either the PDMS base, PDMS with an acrylamide drug-releasing site, or the full device containing PDMS, acrylamide, and doxorubicin. These groups were compared to a control group that underwent incision and suturing without device implantation. The weight of the mice was measured regularly, and blood samples were collected at 0, 7, and 14 days post-implantation for cytokine concentration measurements and immune cell counts.

Cytokine measurements were performed using the LegendPlex Mouse Inflammation Panel (13-plex) (BioLegend) according to the manufacturer's instructions. Samples were acquired using an Aurora spectral flow cytometer (Cytek Biosciences) and analyzed with the LegendPlex Data Analysis Software Suite. To analyze immune cell numbers, blood samples were treated with Fc-block (clone 2.4G2; Bio X Cell) for 5 min at room temperature. Surface staining was then performed for 30 min at 4 °C in the dark. After red blood cell lysis using ammonium chloride lysis buffer, cells were analyzed using the Aurora spectral flow cytometer and FlowJo software (BD Biosciences). The following reagents were used for flow cytometry analysis: FITC-CD3e, FITC-Ly6C, PE-NK1.1, PE-CD11c, PerCP-Cy5.5-CD19, PerCP-Cy5.5-CD11b, PE-Cy7-CD8a, PE-Cy7-MHCII, APC-CD4, APC-F4/80, Alexa Fluor 700-CD45, Alexa Fluor 700-Ly6G, APC-Cy7-CD45, and Zombie NIR Fixable Viability Kit (BioLegend and BD Biosciences).

Mice were euthanized 14 days after device implantation using CO_2 inhalation. Heart, kidney, liver, lung, spleen, and skin tissues were harvested, fixed in 10% neutral-buffered formalin (Biosesang Inc.), and embedded in paraffin wax. Tissue sections were stained with hematoxylin and eosin (H&E) according to the manufacturer's instructions (DeadEnd).

Mechanical Analysis of Hydrogel: All tests were performed in ambient air at room temperature. Hydrogel samples (made following the directions shown above) were prepared in dog-bone-shaped specimens with a gauge width of 10 mm, a gauge length of 10 mm, thickness of 1 mm. Tensile tests were done by Instron (3343, Instron) with a load cell of 50 N. The tensile rate was 10 mm min^{-1} .

DOX Mobility Test: The electrical mobility of DOX in hydrogel was carried out by electrophoresis (Mini-PROTEAN Tetra cell, Bio-Rad). Polycationic double network hydrogel and 3 M acrylamide hydrogel was UV-polymerized in the glass plate (1 mm \times 10 cm \times 8 cm) and immersed in DPBS solution for over 24 h, following the same methodology employed above. Tris-HCl solution (25 mM Tris, pH 7.4) was used as buffer solution and DOX was dissolved in glycerol solution (1 mg mL^{-1} DOX, 10% glycerol in water). CIPN hydrogel was tested under the condition of 71 V for 260 min, applying a constant current of 400 mA. In the case of polyacrylamide hydrogel, an electrophoresis was conducted for 120 min at 179 V with a constant current of 40 mA. During the electrophoresis, the electric field applied to the hydrogels were measured employing a digital multimeter (Fluke 117) connected to both ends of the hydrogel via Ag/AgCl electrodes. Throughout all electrophoretic experiments, the device was maintained at 0 °C by using ice water. The electrical mobility of DOX in aqueous solution was given by Einstein-Smoluchowski relation expressed as

$$\mu_q = \frac{Dq}{k_B T} \quad (2)$$

where μ_q is the electrical mobility ($\mu = \mu_q / q$, ratio of the particles terminal drift velocity to an applied electric field), q is the electrical charge of the ion,

k_B is the Boltzmann constant, and T is the absolute temperature of the ion, respectively.

Electrochemical Analysis of IDDS: Current-Voltage curves of IDDS were recorded with electrochemical analyzer by scanning the voltage from -2.0 to $+2.0$ V at a scan rate of 10 mV s^{-1} . Ag/AgCl electrodes were used as working, reference, and counter electrodes. In all experiments, the Ag/AgCl electrodes inside the drug chamber were the working electrode. DPBS solution was used for the electrolyte solution inside diode-tissue interface. The twisting test was conducted using alligator clips and stretching test was conducted using Instron with a load cell of 50 N during cyclovoltammetry. The current-time curves of IDDS were generated using an electrochemical analyzer. A 5-min period under a $+3.7$ V forward electric bias was followed by a -3.7 V reverse electric bias.

Mechanical Analysis of IDDS: All tests were performed in ambient air at room temperature. The initial dimensions of an IDDS sample were 10 mm \times 10 mm \times 5 mm. Tensile tests were done by Instron (3343, Instron) with a load cell of 50 N. The tensile rate was 10 mm min^{-1} .

Measurement of Drug Delivery Properties: For the accuracy of the measurement, the acrylamide hydrogel of the diode-tissue interface was polymerized in 200 μm . To measure the drug delivery properties of IDDS, two Ag/AgCl electrodes were used under electrical stimuli by electrochemical analyzer (ZIVE MP1, WonATech). Diode-tissue interface was immersed in DPBS solution (20 μL) and then was treated under certain DC voltage (1, 2, 3, 3.7, 4 V). After a certain time (1, 2, 3, 4, 5 min) of the stimuli, DPBS solution was drawn for UV-VIS spectroscopic analysis of the absorption peak at 485 nm (Nanodrop 2000, Thermo Fisher Scientific). Only for Figure S13A (Supporting Information), the absorbance graph was smoothed by Origin analysis tool (Adjacent-averaging, point of window: 20) For the next measurement, the DPBS is refilled in same amount. The total current and charge data was recorded with electrochemical analyzer. To analyze the drug release properties of IDDS at various doxorubicin concentrations, the concentration of doxorubicin within the polyacrylamide hydrogel in the drug chamber was varied at 1, 2, 3, 4, and 5 mg mL^{-1} . All other experimental conditions remained identical to those described earlier.

Cyclic Drug Delivery Test: For cyclic drug delivery test, IDDS was immersed in DPBS solution (500 μL) and then was treated under 3.7 V DC voltage by lithium-polymer battery (YJ701438, YJ Power Group Limited). The drug delivery cycle was composed of sequential phases: a 6 min duration with $+3.7$ V forward bias, followed by a 44 min period of rest at 0 V, then a 55 min interval with -3.7 V reverse bias, succeeded by a 15 min rest period. Each cycle spans a total of 2 h and is managed through a wireless switch (MosMT+TMB-02, YurKuong) and a remote-controlled toggle switch (Fingerbot HSF-SI100, RSH Technology Co., Limited). After a certain cycle of the stimuli, DPBS solution was drawn for UV-vis spectroscopic analysis. The concentration of DOX followed from measurements of the absorption peak at 485 nm. The current-time curves of the cyclic test were measured by electrometer (Electrometer 6517B, KEITHLEY).

In-Vivo Anti-Tumor and Immune Toxicity Analysis of IDDS: B16F10 melanoma cells were purchased from the American Type Culture Collection (ATCC). To establish subcutaneous tumors, 1×10^6 B16F10 cells were injected into the right flank of the mice. Tumors, typically reaching 1 cm in diameter, developed within 1–3 weeks post-injection. Tumors size was regularly measured using digital calipers, and volumes were calculated using the formula: length \times width \times height / 2.

Seven days post-tumor inoculation, skin was excised 1 cm away from tumor mass, and the IDDS was implanted between tumor mass and the peritoneum. The device was programmed to operate on a 2-h cycle, allowing for 6 min of drug release under forward bias and 55 min for electrode recovery under reverse bias. The control group received equivalent doses of DOX per day via direct intratumoral injection.

Ten days after device implantation, mice were euthanized using CO_2 inhalation, and tumor tissues were collected for flow cytometry analysis. Single-cell suspensions were prepared from the tumor tissues using the Mouse Tumor Dissociation Kit (Miltenyi Biotec) and Percoll (GE Healthcare) density gradient separation according to the manufacturer's recommendations.

Typically, up to 1×10^6 cells were treated with Fc-block (2.4G2 clone; Bio X cell) for 5 min at room temperature (RT) and surface staining was

performed for 30 min at 4 °C in the darkness. Cells were analyzed using a Canto II flow cytometer (BD Biosciences), and data were processed using FlowJo software (BD Biosciences). The following antibodies were used for flow cytometry analysis: CD3e-FITC, PerCP-Cy5.5-CD19, PE-Cy7-CD8a, APC-PD-1, Alexa Fluor 700-CD4, APC-Cy7-CD45 (BioLegend), NK1.1-PE, Fixable Viability Stain 620 (BD Biosciences).

Supporting Information

Supporting Information is available from the Wiley Online Library or from the author.

Acknowledgements

National Research Foundation of Korea (NRF) grant funded by the Korean Government (No. 2021R1A2C2092737, No. 2021R1A5A1030054) and the Ministry of Science and ICT (RS-2023-00225581, RS-2023-00219002, RS-2024-00459269, RS-2024-00457721, RS-2023-00219002). The Korea Health Industry Development Institute funded by Ministry of Health and Welfare (HD22C2045). Pioneer Research Center Program through the National Research Foundation of Korea funded by the Ministry of Science, ICT & Future Planning (grant no. NRF-2022M3C1A3081211).

Conflict of Interest

The authors declare no conflict of interest.

Author Contributions

H.Y., S.-B.K., and J.K. contributed equally to this work. H.Y., S.-B.K., J.K. performed conceptualization. H.Y., S.-B.K., J.K., W.C. performed methodology. H.Y., S.-B.K., J.K., W.C., H.H., S.O., H.L., D.-Y.L. performed investigation. H.Y., J.K. performed visualization. T.D.C., K.-M.L., J.-Y.S. performed supervision. H.Y., S.-B.K., J.K. wrote original draft. H.Y., S.-B.K., J.K., W.C., S.-H.J., S.L., C.S.P., and D.-Y.L. wrote, reviewed, and edited.

Data Availability Statement

The data that support the findings of this study are available from the corresponding author upon reasonable request.

Keywords

active drug delivery system, flow-free, hydrogel-based device, immune toxicity, ionic diode

Received: August 21, 2024
Revised: November 29, 2024
Published online: December 24, 2024

- [1] M. W. Tibbitt, J. E. Dahlman, R. Langer, *J. Am. Chem. Soc.* **2016**, *138*, 704.
- [2] F. M. Kashkooli, M. Soltani, M. Souri, *J. Controlled Release* **2020**, *327*, 316.
- [3] S. M. Mirvakili, R. Langer, *Nat. Electron.* **2021**, *4*, 464.

- [4] Y. Zhang, F. Liu, Y. Zhang, J. Wang, D. D'Andrea, J. B. Walters, S. Li, H. J. Yoon, M. Wu, S. Li, Z. Hu, T. Wang, J. Choi, K. Bailey, E. Dempsey, K. Zhao, A. Lantsova, Y. Bouricha, I. Huang, H. Guo, X. Ni, Y. Wu, G. Lee, F. Jiang, Y. Huang, C. K. Franz, J. A. Rogers, *Proc. Natl. Acad. Sci. USA* **2023**, *120*, 2217734120.
- [5] a) A. M. Vargason, A. C. Anselmo, S. Mitragotri, *Nat. Biomed. Eng.* **2021**, *5*, 951; b) A. Kar, N. Ahamad, M. Dewani, L. Awasthi, R. Patil, R. Banerjee, *Biomaterials* **2022**, *283*, 121435; c) Y.-N. Wang, L.-M. Fu, *Microelectron. Eng.* **2018**, *195*, 121.
- [6] a) C. R. Thomas, D. P. Ferris, J.-H. Lee, E. Choi, M. H. Cho, E. S. Kim, J. F. Stoddart, J.-S. Shin, J. Cheon, J. I. Zink, *J. Am. Chem. Soc.* **2010**, *132*, 10623; b) W. Gao, D. Kagan, O. S. Pak, C. Clawson, S. Campuzano, E. Chuluun-Erdene, E. Shipton, E. E. Fullerton, L. Zhang, E. Lauga, *Small* **2012**, *8*, 460.
- [7] a) R. Farra, N. F. Sheppard Jr, L. McCabe, R. M. Neer, J. M. Anderson, J. T. Santini Jr, M. J. Cima, R. Langer, *Sci. Transl. Med.* **2012**, *4*, 122ra121; b) J. Koo, S. B. Kim, Y. S. Choi, Z. Xie, A. J. Bando, K. J. Khalifeh, Y. Yan, H. Kim, M. K. Pezhough, K. Doty, *Sci. Adv.* **2020**, *6*, eabb1093.
- [8] a) S. H. Sung, Y. S. Kim, D. J. Joe, B. H. Mun, B. K. You, D. H. Keum, S. K. Hahn, M. Berggren, D. Kim, K. J. Lee, *Nano Energy* **2018**, *51*, 102; b) C. H. Lee, H. Kim, D. V. Harburg, G. Park, Y. Ma, T. Pan, J. S. Kim, N. Y. Lee, B. H. Kim, K.-I. Jang, *NPG Asia Mater.* **2015**, *7*, e227.
- [9] a) M. B. Yatvin, J. N. Weinstein, W. H. Dennis, R. Blumenthal, *Science* **1978**, *202*, 1290; b) J. Lee, H. R. Cho, G. D. Cha, H. Seo, S. Lee, C. K. Park, J. W. Kim, S. Qiao, L. Wang, D. Kang, T. Kang, T. Ichikawa, J. Kim, H. Lee, W. Lee, S. Kim, S. T. Lee, N. Lu, T. Hyeon, S. H. Choi, D. H. Kim, *Nat. Commun.* **2019**, *10*, 5205.
- [10] a) D. Wu, F. Fei, Q. Zhang, X. Wang, Y. Gong, X. Chen, Y. Zheng, B. Tan, C. Xu, H. Xie, *Sci. Adv.* **2022**, *8*, eabm3381; b) A. M. Kloxin, A. M. Kasko, C. N. Salinas, K. S. Anseth, *Science* **2009**, *324*, 59; c) C. Zhan, W. Wang, J. B. McAlvin, S. Guo, B. P. Timko, C. Santamaria, D. S. Kohane, *Nano Lett.* **2016**, *16*, 177.
- [11] a) R. Avila, C. Li, Y. Xue, J. A. Rogers, Y. Huang, *Proc. Natl. Acad. Sci. USA* **2021**, *118*, 2026405118; b) W. Ouyang, W. Lu, Y. Zhang, Y. Liu, J. U. Kim, H. Shen, Y. Wu, H. Luan, K. Kilner, S. P. Lee, *Nat. Biomed. Eng.* **2023**, *7*, 1252; c) Y. Zhang, D. C. Castro, Y. Han, Y. Wu, H. Guo, Z. Weng, Y. Xue, J. Ausra, X. Wang, R. Li, *Proc. Natl. Acad. Sci. U. S. A.* **2019**, *116*, 21427.
- [12] a) S. H. Lee, Q. Wan, A. Wentworth, I. Ballinger, K. Ishida, J. E. Collins, S. Tamang, H.-W. Huang, C. Li, K. Hess, *Sci. Adv.* **2021**, *7*, eabj4624; b) S. Y. Chin, Y. C. Poh, A.-C. Kohler, J. T. Compton, L. L. Hsu, K. M. Lau, S. Kim, B. W. Lee, F. Y. Lee, S. K. Sia, *Sci. Rob.* **2017**, *2*, eaah6451.
- [13] F. Casanova, P. R. Carney, M. Sarntinoranont, *J. Biomech. Eng.* **2012**, *134*, 041006.
- [14] W. Chen, L. Zhai, S. Zhang, Z. Zhao, Y. Hu, Y. Xiang, H. Liu, Z. Xu, L. Jiang, L. Wen, *Science* **2023**, *382*, 559.
- [15] M. A. Oh, C. I. Shin, M. Kim, J. Kim, C. M. Kang, S. H. Han, J. Y. Sun, S. S. Oh, Y. R. Kim, T. D. Chung, *ACS Appl. Mater. Interfaces* **2021**, *13*, 26748.
- [16] a) F. Jiang, W. C. Poh, J. Chen, D. Gao, F. Jiang, X. Guo, J. Chen, P. S. Lee, *Nat. Commun.* **2022**, *13*, 6669; b) S. H. Han, S. I. Kim, H.-R. Lee, S.-M. Lim, S. Y. Yeon, M.-A. Oh, S. Lee, J.-Y. Sun, Y.-C. Joo, T. D. Chung, *ACS Appl. Mater. Interfaces* **2021**, *13*, 6606.
- [17] T. Arbring Sjöström, M. Berggren, E. O. Gabrielsson, P. Janson, D. J. Poxson, M. Seitanidou, D. T. Simon, *Adv. Mater. Technol.* **2018**, *3*, 1700360.
- [18] X. Huang, X. Y. Kong, L. Wen, L. Jiang, *Adv. Funct. Mater.* **2018**, *28*, 1801079.
- [19] J. H. Han, K. B. Kim, H. C. Kim, T. D. Chung, *Angew. Chem., Int. Ed.* **2009**, *48*, 3830.

- [20] H. Yuk, T. Zhang, G. A. Parada, X. Liu, X. Zhao, *Nat. Commun.* **2016**, 7, 12028.
- [21] M. A. Nejad, P. Umstätter, H. M. Urbassek, *J. Mol. Model.* **2020**, 26, 54.
- [22] X. Shuai, H. Ai, N. Nasongkla, S. Kim, J. Gao, *J. Controlled Release* **2004**, 98, 415.
- [23] S. Mitragotri, P. A. Burke, R. Langer, *Nat. Rev. Drug Discovery* **2014**, 13, 655.
- [24] N. Casares, M. O. Pequignot, A. Tesniere, F. Ghiringhelli, S. Roux, N. Chaput, E. Schmitt, A. Hamai, S. Hervas-Stubbs, M. Obeid, *J. Exp. Med.* **2005**, 202, 1691.
- [25] L. Galluzzi, A. Buqué, O. Kepp, L. Zitvogel, G. Kroemer, *Nat. Rev. Immunol.* **2017**, 17, 97.
- [26] X. Dang, S. C. Ogbu, J. Zhao, L. N. T. Nguyen, D. Cao, L. N. Nguyen, S. Khanal, M. Schank, B. K. C. Thakuri, X. Y. Wu, *Cell Death Dis.* **2020**, 11, 196.
- [27] S. P. Perfetto, P. K. Chattopadhyay, L. Lamoreaux, R. Nguyen, D. Ambrozak, R. A. Koup, M. Roederer, *Cur. Protocol. Cytom.* **2010**, 53, cy0934s53.
- [28] M. H. Schneider, Y. Tran, P. Tabeling, *Langmuir* **2011**, 27, 1232.
- [29] Y. Lee, S. H. Cha, Y.-W. Kim, D. Choi, J.-Y. Sun, *Nat. Commun.* **2018**, 9, 1804.